

Bridging the Sim-to-real Gap: A Control Framework for Imitation Learning of Model Predictive Control

Seungtaek Kim[✉], Jonghyup Lee[✉], Kyoungseok Han^{*}, and Seibum B. Choi^{*}

Abstract: To address the computational challenges of Model Predictive Control (MPC), recent research has studied using imitation learning to approximate the MPC to a computationally efficient Deep Neural Network (DNN). However, this introduces a common issue in learning-based control, the simulation-to-reality (sim-to-real) gap, and Domain Randomization (DR) has been widely used to mitigate this gap by introducing perturbations in the source domain. However, DR inevitably leads to low data collection efficiency and an overly conservative control strategy. This study proposes a new control framework that addresses this issue from a control perspective inspired by Robust Tube MPC. The framework ensures the DNN operates in the same environment as the source domain, handling the sim-to-real gap with great data collection efficiency. Moreover, a parameter governor is introduced to address the DNN's inability to adapt to variations in model parameters, enabling the system to satisfy MPC constraints more robustly under changing conditions. The proposed framework was validated through two case studies: cart-pole control and vehicle collision avoidance control, which analyzed the principles of the proposed framework in detail and demonstrated its application to a vehicle control case.

Keywords: Imitation Learning, Model Predictive Control, Robust Tube Model Predictive Control, Sim-to-real Gap

1. INTRODUCTION

Model Predictive Control (MPC) has been widely applied in control fields due to its ability to compute the optimal control input while satisfying system constraints [1]. To further enhance its practicality, many studies have focused on reducing its high computational cost. One approach is to approximate MPC with a computationally efficient Deep Neural Network (DNN) using imitation learning [2]. This method involves collecting demonstrations from MPC and training a DNN to imitate its behavior through supervised learning. Studies have shown that this method works effectively, verified by robot gait control [3], drone [4] and vehicle control [5, 6], reducing MPC's computational load by at least 10 to 20 times while maintaining its control performance.

However, applying imitation learning introduces the simulation-to-reality (sim-to-real) gap inevitably, a major issue in the learning-based control area. This gap refers to the disparity between the source domain (where the training data for a DNN is collected, such as simulation or lab) and the target domain (where the DNN is applied in the

real world). Since collecting MPC demonstrations in the real world is impractical, many studies have gathered them in a simulated environment instead, which inherently creates the sim-to-real gap. If this gap is not addressed before applying the DNN to the target domain, the DNN may encounter untrained states, leading to unintended control failures.

Transfer learning techniques [7] have been developed in learning-based control to address the sim-to-real gap, including domain adaptation [8], system identification [9], and Domain Randomization (DR). Among these, DR has been widely used in control applications that apply random perturbations, such as model parameters and frictions [10], winds [11], noises [12], and visual randomizations [13, 14] in the source domain to make it encompass the target domain. However, several drawbacks still remain: (1) determining which factors to randomize and how to do so is challenging, (2) the amount of training data increases drastically as more random factors are considered, (3) the controller becomes excessively conservative to account for all random variations, and (4) despite these efforts, the randomized elements may not fully capture the

Manuscript received XX XX, XXXX; This work was supported by the BK21 FOUR Program of the National Research Foundation Korea (NRF) grant funded by the Ministry of Education (MOE), the Korea government (MSIT), Ministry of Trade, Industry and Energy (MOTIE, Korea), and Korea Evaluation Institute of Industrial Technology (KEIT). (No. RS-2024-00346702, No. 20023815, and No. 20018181)

Seungtaek Kim and Seibum B. Choi (Corresponding Author) are with the Dept. of Mechanical Engineering, Korea Advanced Institute of Science and Technology, Daejeon 34141, South Korea (email: kimst9o9@kaist.ac.kr, sbchoi@kaist.ac.kr). Jonghyup Lee is with the Dept. of Mechanical Systems Engineering, Sookmyung Women's University, Seoul 04310, South Korea (email: jhyuplee@sookmyung.ac.kr). Kyoungseok Han (Co-corresponding Author) is with the Dept. of Automotive Engineering, Hanyang University, Seoul 04763, South Korea (email: kyoungsh@hanyang.ac.kr).

* Corresponding authors.

gap, making the DNN still vulnerable to sim-to-real gap.

Various studies have been conducted to overcome these limitations of DR. A study applied the concept of bounded error tube as a criterion for randomizing factors [15], and to further improve data collection efficiency, a method for extracting samples from each vertex or face of a polytope error tube was proposed [16]. However, these approaches still required additional perturbed data and resulted in a conservative control strategy as other DR methods. To address parameter changes that may occur in the target domain, a parameter-adaptive approximate MPC [17] was proposed, which attaches a linear predictor that compensates for the parameter changes to the DNN controller. However, a significant amount of MPC demonstrations was still required to overcome the remaining sim-to-real gap.

This study, on the other hand, proposes a new control framework that overcomes the limitations (1) - (4) of existing DR methods. While previous approaches focus on directly reducing the sim-to-real gap, our method addresses the issue from a control perspective. Inspired by Robust Tube MPC (RTMPC) structure and [16], the proposed framework configures the approximate DNN as a nominal controller that only controls the nominal model, ensuring it only operates within the state distribution of the source domain. This prevents instability caused by the sim-to-real gap, as the DNN is prevented from being exposed to an untrained state. Because the DNN acts as a feedforward controller, which only controls the nominal model, a stable ancillary controller is introduced to guide the actual plant in following the nominal model controlled by the DNN. Furthermore, a parameter governor [18], which is an add-on component, refines the control inputs from both controllers, allowing the controller to adapt to changes in plant model parameters that the DNN alone cannot handle, enforcing to satisfy MPC constraints and allowing for a less conservative MPC to be imitated. To validate the proposed framework, two case studies were conducted, cart-pole and vehicle collision avoidance systems, providing a detailed explanation of its components and demonstrating its superior performance in handling the sim-to-real gap compared to existing DR methods.

The key contributions of the proposed framework are as follows:

- 1) Unlike DR, it avoids the need to introduce random factors in the source domain during MPC demonstration collection, making data collection more efficient.
- 2) There is no need to design a high-fidelity simulation for the source domain because the proposed nominal model-based source domain is already obtained from the MPC design process.
- 3) By adapting to plant parameter changes, the framework allows for a less conservative MPC to be imitated, improving the overall control performance.

The remainder of this paper is organized as follows: Section II presents the problem statement of the sim-to-real gap in applying imitation learning to MPC. Section III details the proposed control framework. Section IV presents the case study of the proposed framework using a cart-pole and vehicle collision avoidance systems, followed by the conclusion and future work provided in Section V.

2. PROBLEM STATEMENT

This section explains the process of applying imitation learning to MPC and where the sim-to-real gap occurs.

2.1. Imitation learning of model predictive control

The MPC's optimization problem calculates the optimal control input sequence $U^*(k) = [u_{0|k}^*, u_{1|k}^*, \dots, u_{N-1|k}^*]^T$, minimizing the cost function with the constraint satisfaction over the prediction horizon as follows:

$$\min_{U(k)} J(x(k), U(k)) \quad (1a)$$

$$\text{subject to } x_{i+1|k} = f(x_{i|k}, u_{i|k}, \bar{M}) \quad (1b)$$

$$x_{i|k} \in \mathbb{X}, u_{i|k} \in \mathbb{U}, x_{N|k} \in \mathbb{X}_f \quad (1c)$$

$$x_{0|k} = x(k) \quad (1d)$$

$$\text{for } i = 0, \dots, N-1 \quad (1e)$$

where J is the cost function, f is the nominal prediction model, \bar{M} denotes nominal model parameters, and x, u are the control state and input, respectively; $(\bullet)_{i|k}$ denotes the predicted value in step $k+i$ made in step k ; N is the prediction horizon; and \mathbb{X}, \mathbb{U} , and \mathbb{X}_f are the constraint sets of the state and input. The first element of the optimized input sequence is then used as the resultant control input u_{MPC} at step k :

$$u_{\text{MPC}}(x(k)) = u_{0|k}^*. \quad (2)$$

Applying imitation learning to approximate MPC is to find the parameter θ of the DNN π_θ that imitates MPC by minimizing the expected error between u_{MPC} and π_θ in the target domain \mathcal{T} . By using the MPC's demonstrations in \mathcal{T} , θ is estimated as $\theta_{\mathcal{T}}^*$ through supervised learning with the widely used mean squared error loss function \mathcal{L} :

$$\theta_{\mathcal{T}}^* = \underset{\theta}{\operatorname{argmin}} \mathbb{E}_{p(\xi|u_{\text{MPC}}, \mathcal{T})} [\mathcal{L}(\xi, \theta)] \quad (3a)$$

$$\mathcal{L}(\xi, \theta) = \frac{1}{L_T} \sum_{k=0}^{L_T-1} \|u_{\text{MPC}}(x(k)) - \pi_\theta(x(k))\|_2^2 \quad (3b)$$

where $\xi = [x(0), x(1), \dots, x(L_T-1)]$ is the state trajectory driven by u_{MPC} in \mathcal{T} , and $p(\xi|u_{\text{MPC}}, \mathcal{T})$ is the probability distribution of ξ .

However, due to the difficulty in gathering MPC demonstrations in the target domain \mathcal{T} , a high-fidelity simulation, which is called the source domain \mathcal{S} , has been

accessed to gather them. Then, $\theta_{\mathcal{T}}^*$ is instead estimated as $\theta_{\mathcal{S}}^*$:

$$\theta_{\mathcal{S}}^* = \underset{\theta}{\operatorname{argmin}} \mathbb{E}_{p(\xi|u_{\text{MPC}}, \mathcal{S})} [\mathcal{L}(\xi, \theta)]. \quad (4)$$

2.2. Sim-to-real gap

This approach leads to the covariate shift problem due to the discrepancy between \mathcal{T} and \mathcal{S} that can be expressed as follows [16]:

$$\mathbb{E}_{p(\xi|u_{\text{MPC}}, \mathcal{T})} [\mathcal{L}(\xi, \theta_{\mathcal{S}}^*)] - \mathbb{E}_{p(\xi|u_{\text{MPC}}, \mathcal{S})} [\mathcal{L}(\xi, \theta_{\mathcal{S}}^*)]. \quad (5)$$

The above quantity indicates that the approximate DNN would not guarantee the designed performance in the target domain because it can encounter untrained states, which is commonly referred to as the sim-to-real gap problem.

Therefore, attempts to make the source domain encompass the target domain have been made, such as applying random disturbances or sampling perturbations $d \sim p_{\mathcal{T}}(d)$ in the source domain, namely DR. The approximate DNN $\theta_{\mathcal{S},d}^*$ is then found as follows:

$$\theta_{\mathcal{S},d}^* = \underset{\theta}{\operatorname{argmin}} \mathbb{E}_{p_{\mathcal{T}}(d)} [\mathbb{E}_{p(\xi|u_{\text{MPC}}, \mathcal{S}, d)} [\mathcal{L}(\xi, \theta)]] \quad (6)$$

with the probability distribution $p(\xi|u_{\text{MPC}}, \mathcal{S}, d)$ denoting the transition probability driven by u_{MPC} in \mathcal{S} under random perturbations d . Although DR helps mitigate the sim-to-real gap, it is challenging to determine the appropriate type and magnitude of perturbations. Additionally, as the level of perturbation increases, the amount and complexity of required training data grow significantly.

3. PROPOSED CONTROL FRAMEWORK

This section briefly reviews the RTMPC and explains the proposed control framework which is inspired by the RTMPC. Details on RTMPC can be referred to [19].

3.1. Brief review of RTMPC

RTMPC is the same as the MPC but ensures the satisfaction of the designed constraints \mathbb{X} , \mathbb{U} , and \mathbb{X}_f even for the system with disturbances:

$$x(k+1) = f(x(k), u(k), \bar{M}) + w(k). \quad (7)$$

Its optimization problem computes a conservative optimal control input sequence $\bar{U}^*(k) = [\bar{u}_{0|k}^*, \bar{u}_{1|k}^*, \dots, \bar{u}_{N-1|k}^*]^T$, which minimizes the cost function while satisfying tightened constraints $\bar{\mathbb{X}}$, $\bar{\mathbb{U}}$, and $\bar{\mathbb{X}}_f$:

$$\min_{\bar{U}(k)} J(\bar{x}(k), \bar{U}(k)) \quad (8a)$$

$$\text{subject to } \bar{x}_{i+1|k} = f(\bar{x}_{i|k}, \bar{u}_{i|k}, \bar{M}) \quad (8b)$$

$$\bar{x}_{i|k} \in \bar{\mathbb{X}}, \bar{u}_{i|k} \in \bar{\mathbb{U}}, \bar{x}_{N|k} \in \bar{\mathbb{X}}_f \quad (8c)$$

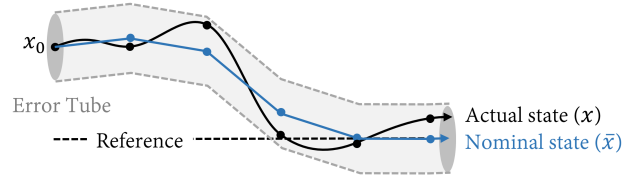


Fig. 1. RTMPC concept.

$$\bar{x}_{0|k} = \bar{x}(k) \quad (8d)$$

$$\text{for } i = 0, \dots, N-1 \quad (8e)$$

Notably, the RTNMPC's optimization problem considers only the nominal state \bar{x} , as shown in (8d), and calculates the nominal control input using the first element of $\bar{U}^*(k)$ as follows:

$$u_{\text{MPC}}(\bar{x}(k)) = \bar{u}_{0|k}^*. \quad (9)$$

with the nominal state propagated by the nominal model:

$$\bar{x}(k+1) = f(\bar{x}(k), u_{\text{MPC}}(\bar{x}(k)), \bar{M}) \quad (10a)$$

$$\bar{x}(0) = x(0). \quad (10b)$$

Because the nominal controller $u_{\text{MPC}}(\bar{x}(k))$ controls only the nominal state, the actual state propagates differently from the nominal state due to disturbances present in the system (7). Hence, RTNMPC includes not only $u_{\text{MPC}}(\bar{x}(k))$ but also the following control input $\kappa(x(k), \bar{x}(k))$:

$$u_{\text{RTMPC}}(x(k)) = u_{\text{MPC}}(\bar{x}(k)) + \kappa(x(k), \bar{x}(k)). \quad (11)$$

The term $\kappa(x(k), \bar{x}(k))$ is a stable feedback or so-called ancillary controller that regulates the error between the nominal state \bar{x} and the actual state x , resulting in the following error dynamics for $e(k) = x(k) - \bar{x}(k)$:

$$e(k+1) = \Phi(k)e(k) + w(k) \quad (12)$$

Note that the overall RTMPC becomes stable when both nominal and ancillary controllers are stable. A typical method to design an ancillary controller is to design it as a full-state feedback controller [20]:

$$\kappa(x(k), \bar{x}(k)) = K(x(k) - \bar{x}(k)) \quad (13)$$

where K is set to make the linearized error dynamics for $e(k)$:

$$e(k+1) \approx (A(k) + B(k)K)e(k) + w(k) \quad (14)$$

Hurwitz-stable with all the possible linearized system matrices $A(k) = \nabla_x f|_{\bar{x}(k), \bar{u}(k), \bar{M}}$ and $B(k) = \nabla_u f|_{\bar{x}(k), \bar{u}(k), \bar{M}}$, assuming linearization errors are negligible.

Fig. 1 illustrates the concept of RTMPC. The nominal controller controls the nominal state toward the reference,

while the ancillary controller keeps the actual state within a region around it, also known as the error tube. Here, the size of the error tube is considered to tighten the original constraints for the optimization problem to ensure the actual states satisfy the original constraints.

3.2. Nominal and ancillary controllers

The key concept of RTMPC that inspired this study is that the nominal controller operates solely on the nominal state \bar{x} , while the ancillary controller compensates for the error between nominal state \bar{x} and the actual state x . This suggests that if the DNN controller, approximating MPC, functions as the nominal controller, it only requires information from the nominal state distribution for training. Based on this idea, this study proposes the following definition and proposition.

Definition 1 Nominal model-based domain \mathcal{S}_{nom} : A domain \mathcal{S}_{nom} in which the state x is propagated by the nominal model, as the following equation, is called the nominal model-based domain \mathcal{S}_{nom} .

$$x(k+1) = f(x(k), u(k), \bar{M}) \quad (15)$$

Proposition 1: If the DNN π_θ , approximating the MPC is composed as a nominal controller in the overall control structure attached with an ancillary controller as follows:

$$u(k) = \pi_\theta(\bar{x}(k)) + \kappa(x(k), \bar{x}(k)), \quad (16)$$

where \bar{x} is the nominal state propagated by the nominal model, and x is the actual state, then the target domain of the DNN controller becomes equal to the nominal model-based domain \mathcal{S}_{nom} .

Proof: The proof is trivial as the nominal DNN controller π_θ only receives the nominal state \bar{x} . \square

That is, in the proposed framework, the DNN, which approximates MPC, serves as the nominal controller and is responsible only for controlling the nominal state, and the ancillary controller ensures that the actual state follows the nominal state, leaving the error dynamics between them same as (12) but with $\bar{u}(k) = \pi_\theta(\bar{x}(k))$. Note that $w(k)$ represents the disturbance caused by the sim-to-real gap, indicating the discrepancy of the state propagations between the source domain (nominal state) and the target domain (actual state).

The key idea is that the DNN receives only the nominal state, making its target domain the same as the nominal model-based domain \mathcal{S}_{nom} . As a result, training the DNN to approximate MPC requires only MPC demonstrations from \mathcal{S}_{nom} , without the need to access the full target domain \mathcal{T} . This approach enables effective imitation learning for MPC while eliminating the challenges caused by the sim-to-real gap. Therefore, using MPC demonstrations

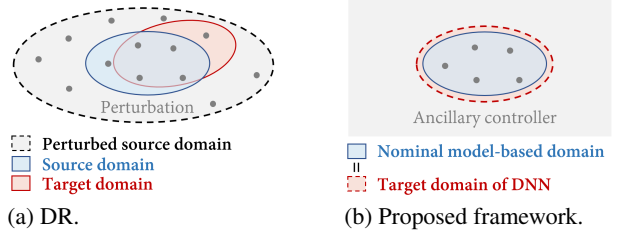


Fig. 2. Diagrams representing (a) Domain Randomization (DR) and (b) the proposed framework.

in \mathcal{S}_{nom} , θ can be obtained as $\theta_{\mathcal{S}_{\text{nom}}}^*$ through supervised learning:

$$\theta_{\mathcal{S}_{\text{nom}}}^* = \underset{\theta}{\operatorname{argmin}} \mathbb{E}_{p(\bar{\xi} | u_{\text{MPC}}, \mathcal{S}_{\text{nom}})} [\mathcal{L}(\bar{\xi}, \theta)] \quad (17a)$$

$$\mathcal{L}(\bar{\xi}, \theta) = \frac{1}{L_T} \sum_{k=0}^{L_T-1} \|u_{\text{MPC}}(\bar{x}(k)) - \pi_\theta(\bar{x}(k))\|_2^2 \quad (17b)$$

where $\bar{\xi} = [\bar{x}(0), \bar{x}(1), \dots, \bar{x}(L_T-1)]$ is the nominal state trajectory driven in \mathcal{S}_{nom} by u_{MPC} , and $p(\bar{\xi} | u_{\text{MPC}}, \mathcal{S}_{\text{nom}})$ is the probability distribution of $\bar{\xi}$ in \mathcal{S}_{nom} .

Unlike DR, this approach does not require sampling perturbations around the source domain to address the sim-to-real gap, significantly improving data collection efficiency. Moreover, there is no need to create a high-fidelity simulation that closely matches the target domain since the nominal model used in \mathcal{S}_{nom} is already available from the MPC design process. Fig. 2 compares DR and the proposed framework. While DR introduces perturbations in the source domain (Fig. 2a) to encompass the target domain, the proposed method redefines the DNN's target domain as the nominal model-based domain (Fig. 2b).

3.3. Parameter governor

The sim-to-real gap requires the constraints of the imitated MPC to be conservatively tightened to ensure the actual states satisfy the original constraints, which is not limited to our proposed framework but also the same to other transfer learning techniques. However, a key limitation of imitation learning is that once a DNN approximates the controller, it is hard to adapt to changes in the plant's model parameters. Therefore, varying parameters should also be treated as disturbances, leading to overly conservative constraints.

To address this, a parameter governor, which is an add-on component in the proposed framework, is proposed that refines the control input from u to u^* based on updated model parameters instead of the DNN controller. This allows for a less conservative constraint design, ultimately enhancing overall control performance.

The original constraint sets \mathbb{X} and \mathbb{U} can be integrated

to \mathbb{Y} , defined by the following function $g(\bullet)$:

$$\mathbb{Y} = \mathbb{X} \times \mathbb{U} := \{(x, u) \mid g(x, u, M) \leq 0\} \quad (18)$$

where M represents the plant's changed model parameters. The tightened constraint set is then defined using the constraint tightening parameter $\gamma \geq 0$, as follows:

$$\tilde{\mathbb{Y}} = \tilde{\mathbb{X}} \times \tilde{\mathbb{U}} := \{(\bar{x}, \bar{u}) \mid g(\bar{x}, \bar{u}, \bar{M}) \leq -\gamma\}. \quad (19)$$

Note that the imitated MPC only guarantees the tightened constraints to be satisfied for the nominal states, and therefore, the nominal model parameter \bar{M} is applied in the tightened constraints.

γ can be obtained by subtracting the tightening set \mathbb{Y}_{S_∞} from the original constraint set using Pontryagin set difference \ominus [21]:

$$\tilde{\mathbb{Y}} = \mathbb{Y} \ominus \mathbb{Y}_{S_\infty}. \quad (20)$$

Referring to [19], the tightening set \mathbb{Y}_{S_∞} is determined by the upper bound of the difference between the left-hand sides of the inequalities in (18) and (19). This means that the constraint should be conservatively set based on the resulting difference in $g(\bullet)$.

For the case without using the proposed governor, which is not yet introduced, the error between those values is defined as $e_g(k)$:

$$e_g(k) = g(x(k), u(k), M) - g(\bar{x}(k), \bar{u}(k), \bar{M}) \quad (21)$$

where $\bar{u}(k)$ stands for $\pi_\theta(\bar{x}(k))$, for simplicity. The above equation can be linearized as:

$$e_g(k) \approx C(k)e(k) + D(k)\kappa(x(k), \bar{x}(k)) + w_M(k) + w_{\pi_\theta}(k) \quad (22)$$

with $e(k) = x(k) - \bar{x}(k)$; linearized matrices $C(k) = \nabla_x g|_{\bar{x}(k), \bar{u}(k), \bar{M}}$, $D(k) = \nabla_u g|_{\bar{x}(k), \bar{u}(k), \bar{M}}$; and $w_M(k)$ denoting the disturbance caused by model parameter variations:

$$w_M(k) = \nabla_M g|_{\bar{x}(k), \bar{u}(k), \bar{M}}(M - \bar{M}). \quad (23)$$

and $w_{\pi_\theta}(k)$ denoting the disturbance caused by DNN approximation errors:

$$w_{\pi_\theta}(k) = \nabla_u g|_{\bar{x}(k), \bar{u}(k), \bar{M}}(\pi_\theta(\bar{x}(k)) - u_{\text{MPC}}(\bar{x}(k))). \quad (24)$$

(22) represents the linearized constraint violation per time step, and by accumulating these values over the infinite time horizon, the tightening set \mathbb{Y}_{S_∞} is obtained as follows using the Minkowski sum \oplus [21]:

$$\mathbb{Y}_{S_\infty} \approx \bigcup_{n=0}^{\infty} \bigoplus_{k=n}^{\infty} (C(k)\mathbb{S}_{n,k} \oplus D(k)\mathbb{K}) \oplus \mathbb{W}_M \oplus \mathbb{W}_{\pi_\theta} \quad (25)$$

where \mathbb{W}_M and \mathbb{W}_{π_θ} are the set for $w_M(k)$ and $w_{\pi_\theta}(k)$, respectively, \mathbb{K} is the set for the ancillary controller

$\kappa(x(k), \bar{x}(k))$ and $\mathbb{S}_{n,k}$ is the propagated error tube of $e(k)$ from step n to k :

$$\mathbb{S}_{n,k} \approx \bigoplus_n^k \Phi(n)^{k-n} \mathbb{W}, \quad (26)$$

derived from (12) with \mathbb{W} representing the disturbance set for $w(k)$. Note that the approximation symbols (\approx) arise from linearization errors, which this study assumes to be negligibly small.

Referring to (25), the tightening set \mathbb{Y}_{S_∞} includes the set \mathbb{W}_M which is caused by model parameter variations and makes the constraint overly conservative. Therefore, to cancel out the tightening component \mathbb{W}_M , this study proposes the following parameter governor with propositions and assumptions.

Proposition 2: Under the control structure of Proposition 1, if the control input $u(k)$ is refined as $u^*(k)$ that satisfies the following condition:

$$g(x(k), u^*(k), M) = g(\bar{x}(k), u(k), \bar{M}), \quad (27)$$

where $g(\bullet)$ is the function in (18); $x(k)$ is the actual state; $\bar{x}(k)$ is the nominal state; M is the updated plant model parameters; \bar{M} is the nominal model parameters; $u(k)$ is the resultant control input from Proposition 1, then the tightening set \mathbb{W}_M caused by model parameter variations is canceled out.

Proof: Since the refined control input $u^*(k)$ is applied, the tightening set $\mathbb{Y}_{S_\infty}^*$ can be redefined as the upper bound of the following difference:

$$e_g^*(k) = g(x(k), u^*(k), M) - g(\bar{x}(k), \bar{u}(k), \bar{M}), \quad (28)$$

which can be rearranged as follows by applying (27):

$$e_g^*(k) = g(\bar{x}(k), u(k), \bar{M}) - g(\bar{x}(k), \bar{u}(k), \bar{M}) \quad (29)$$

Therefore, the above equation can be linearized as:

$$e_g^*(k) \approx D(k)\kappa(x(k), \bar{x}(k)) + w_{\pi_\theta}(k). \quad (30)$$

Then, the tightening set \mathbb{Y}_{S_∞} can be derived as:

$$\mathbb{Y}_{S_\infty}^* \approx \bigcup_n \bigoplus_{k=n}^{\infty} D(k)\mathbb{K}^* \oplus \mathbb{W}_{\pi_\theta} \quad (31)$$

where \mathbb{K}^* is the new set for the ancillary controller $\kappa(x(k), \bar{x}(k))$ when refined input u^* is applied. Accordingly, as shown in (31), the effect of model parameter variations \mathbb{W}_M is canceled out from the tightening set (25). \square

Followed by some assumptions, it is shown that the required tightening set is reduced when applying the proposed parameter governor under model parameter changes.

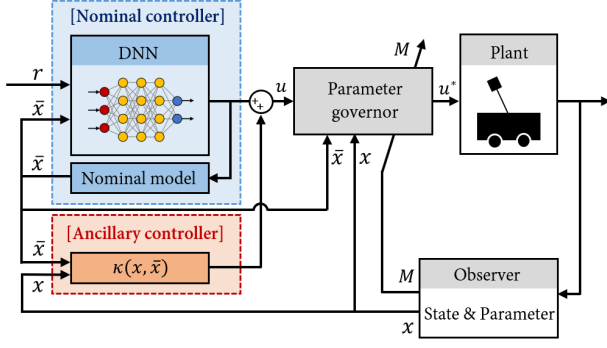


Fig. 3. The overall structure of the proposed control framework. The DNN controller is composed as a nominal controller, operating within the same environment as the source domain S_{nom} . An ancillary controller ensures that the actual plant follows the nominal model, while a parameter governor refines the control input to handle model parameter variations.

Proposition 3: If the refined input $u^*(k)$, derived from Proposition 2, reduces the new ancillary controller set \mathbb{K}^* when applying $u^*(k)$ instead of $u(k)$, meaning:

$$\mathbb{K}^* \subseteq \mathbb{K}. \quad (32)$$

and the linearization errors for $A(k)$, $B(k)$, $C(k)$, and $D(k)$ are negligibly small, then the tightening set $\mathbb{Y}_{S_{\infty}}^*$ resulting from the refined control input $u^*(k)$, defined in Proposition 2, is the subset of $\mathbb{Y}_{S_{\infty}}$:

$$\mathbb{Y}_{S_{\infty}}^* \subseteq \mathbb{Y}_{S_{\infty}} \quad (33)$$

Proof: Define $\tilde{\mathbb{Y}}_{S_{\infty}}$ as an intermediate tightening set as follows:

$$\tilde{\mathbb{Y}}_{S_{\infty}} = \bigcup_n \bigoplus_{k=n}^{\infty} D(k) \mathbb{K} \oplus \mathbb{W}_{\pi_{\theta}}. \quad (34)$$

The following inclusion holds because $\mathbb{K}^* \subseteq \mathbb{K}$:

$$\mathbb{Y}_{S_{\infty}}^* \subseteq \tilde{\mathbb{Y}}_{S_{\infty}} \quad (35)$$

Also, because the terms $S_{n,k}$ and \mathbb{W}_M are included in $\mathbb{Y}_{S_{\infty}}$ compared to $\tilde{\mathbb{Y}}_{S_{\infty}}$, the following inclusion holds:

$$\tilde{\mathbb{Y}}_{S_{\infty}} \subseteq \mathbb{Y}_{S_{\infty}} \quad (36)$$

By (35) and (36), it is confirmed that $\mathbb{Y}_{S_{\infty}}^*$ is a subset of $\mathbb{Y}_{S_{\infty}}$, meaning that the required tightening set $\mathbb{Y}_{S_{\infty}}^*$ is reduced from $\mathbb{Y}_{S_{\infty}}$. \square

In summary, the proposed governor refines the control input based on the updated model parameters, using (27) instead of the DNN controller. This enables a less conservative MPC to be approximated to the DNN while ensuring that MPC constraints remain robustly satisfied even under model parameter variations.

Practically, (32) can also be thought as the following condition:

$$\mathbb{W}^* \subseteq \mathbb{W}. \quad (37)$$

where \mathbb{W}^* represents the new disturbance set for the discrepancy $w^*(k)$ between the plant and the nominal model when applying the refined input $u^*(k)$ to the plant:

$$x(k+1) = f(x(k), u(k), \bar{M}) + w^*(k). \quad (38)$$

(37) means that the refined input makes the behavior of the plant closer to that of the nominal model, which naturally reduces the magnitude of the ancillary controller ($\mathbb{K}^* \subseteq \mathbb{K}$). Therefore, condition (37) can be used instead for the (32) when designing the governor, as it is more intuitively interpretable.

3.4. Remark

Fig. 3 illustrates the overall structure of the proposed control framework. It is important to note that the proposed structure does not eliminate the physical differences between the source and target domains. Instead, these differences remain and are compensated for by the ancillary controller, allowing the DNN to operate solely in the source domain. In other words, the sim-to-real gap is no longer a "problem directly addressed by the neural network" but a "problem managed by the ancillary controller."

However, this framework assumes the ancillary controller and governor can be successfully constructed, which may not hold for highly nonlinear or underactuated systems. Especially designing a governor that meets the aforementioned propositions and assumptions can be challenging. Therefore, to provide insight into its practical implementation, this study presents two case studies, offering a pathway for generalizing the proposed framework to other control problems.

4. CASE STUDY

The proposed control framework was validated in two case studies: cart-pole control and vehicle collision avoidance control. Each for analyzing the principles of the proposed framework in detail and showing the results of applying it to a practical vehicle control case, respectively.

4.1. Cart-pole system

For the cart-pole system, shown in Fig. 4, the control objective is to regulate both cart position and pole angle to the origin while ensuring the wheel force does not exceed the friction limit. To achieve this, an MPC was designed, followed by imitation learning, and applied to the proposed control framework.

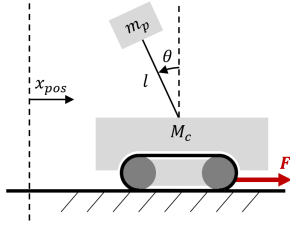


Fig. 4. Cart-pole system.

The system dynamics for the cart-pole is given by:

$$\ddot{x}_{\text{pos}} = \frac{F - (m_p l \dot{\theta}^2 - m_p g \cos \theta) \sin \theta}{M_c + m_p \sin^2 \theta} \quad (39a)$$

$$\ddot{\theta} = \frac{\cos \theta (F - (m_p l \dot{\theta}^2 - (M_c + m_p) g) \sin \theta)}{l(M_c + m_p \sin^2 \theta)} \quad (39b)$$

where x_{pos} is the cart position, θ is the pole angle, M_c and m_p are cart and pole masses, l is the pole length, and g is the gravitational acceleration. F is the control input representing the force applied by the cart's wheel. The system can be represented by the state $x = [x_{\text{pos}}, \dot{x}_{\text{pos}}, \theta, \dot{\theta}]^T$, control input $u = F$, and model parameters $M = [M_c, m_p]$.

The control objective is to regulate both x_{pos} and θ to the origin from $x(0) = [3, 0, 0, 0]^T$ while ensuring the wheel force does not exceed the friction limit. To formulate the MPC's optimization problem, the nominal prediction model was made as follows:

$$x(k+1) = f(x(k), u(k), \bar{M}) \quad (40)$$

which was derived from (39) and discretized using the 4th-order Runge-Kutta method. The nominal model parameter was set as $\bar{M} = [4\text{kg}, 1\text{kg}]$. A cost function penalizing the states and excessive control inputs was composed as:

$$J(x(k), U(k)) = \sum_{i=0}^{N-1} (x_{i|k}^T Q x_{i|k} + u_{i|k}^T R u_{i|k}) \quad (41)$$

with the horizon of $N = 50$ and $Q = \text{diag}([20, 0, 5, 0])$, $R = 0.001$. Finally, constraints that prevent the wheel force from exceeding the friction limit were formulated as follows:

$$\bar{\mathbf{Y}} = \bar{\mathbf{X}} \times \bar{\mathbf{U}} = \{(\bar{x}, \bar{u}) \mid \left| \frac{F}{\mu F_z} \right| - 1 \leq -\gamma\} \quad (42)$$

where the normal force F_z is given by:

$$F_z(x, u, M) = M_c g + m_p (g - l(\ddot{\theta} \sin \theta + \dot{\theta}^2 \cos \theta)) \quad (43)$$

with road friction $\mu = 0.5$. The tightening parameter was set as $\gamma = 0.2$, which is derived in detail later.

4.1.1 Proposed control framework

By imitation learning, the designed MPC was approximated to a fully connected DNN using supervised learning, with 4 hidden layers of 17 nodes each, and implemented into the proposed framework. Because the goal of this case study is to verify the proposed framework's performance of handling the sim-to-real gap with great data collection efficiency, only a single MPC-demonstrated trajectory $\bar{\xi}$ was collected from \mathcal{S}_{nom} , starting from the initial state $x(0) = [3, 0, 0, 0]^T$ to the origin for 100 steps.

The ancillary controller was designed as a full-state feedback controller, with the typical Linear Quadratic Regulator (LQR) gain $K = [5.7, 10.3, -139.9, -41.7]$ obtained by solving the Discrete Algebraic Riccati Equation (DARE) for the linearized model equation at the origin. Under the proposed framework, the control input $u(k)$ was formulated as:

$$u(k) = \pi_{\theta_{\mathcal{S}_{\text{nom}}}}(\bar{x}(k)) + K(x(k) - \bar{x}(k)) \quad (44)$$

Finally, for the parameter governor, Proposition 2 leads to the following form regarding the friction limit constraints (42):

$$g_{\text{Fr.}}(x(k), u^*(k), M) = g_{\text{Fr.}}(\bar{x}(k), u(k), \bar{M}) \quad (45)$$

where $g_{\text{Fr.}}(\bullet)$ is defined as follows:

$$g_{\text{Fr.}}(x(k), u(k), M) = \left| \frac{u(k)}{\mu F_z(x(k), u(k), M)} \right| - 1 \quad (46)$$

Then, the refined input u^* satisfying (45) can be calculated by the following equation:

$$u^*(k) = u(k) \times \frac{F_z(x(k), u^*(k), M)}{F_z(\bar{x}(k), u(k), \bar{M})} \quad (47)$$

which can be physically interpreted as refining the wheel force proportionally to changes in the normal force; that is, if the cart's mass increases, the force input is also increased accordingly. Intuitively, it can be expected to satisfy (37), as it refines the control input matching the changed mass, which will be shown by graphs later.

The Cart-pole was controlled in the target domain, where a disturbance d within the range of $[-5, 5]$ was randomly applied to the control input ($F = u + d$), creating a gap from the source domain. The model parameter M of the cart-pole was set the same as the nominal ones \bar{M} , while the case under model parameter variations is introduced later.

DR baselines were chosen to be compared with the proposed control framework, including conventional DR method [13] and recently proposed tube-based DR [16]. To compare under the same conditions, both baselines approximated the RTMPC controller:

$$u_{\text{RTMPC}}(x(k)) = u_{\text{MPC}}(\bar{x}(k)) + K(x(k) - \bar{x}(k)), \quad (48)$$

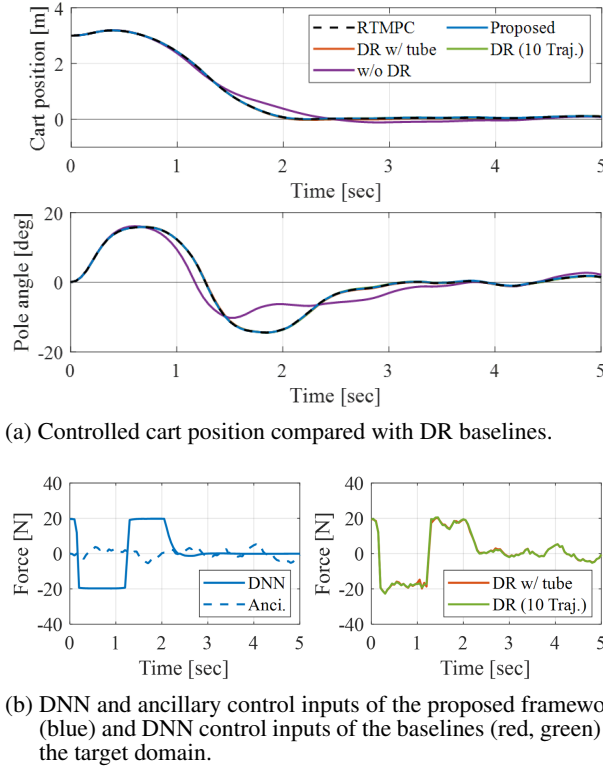


Fig. 5. Controlled cart position and the control inputs in the target domain.

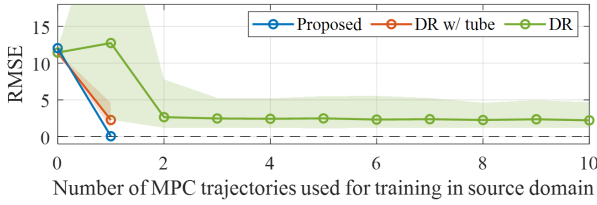


Fig. 6. Root Mean Squared Error (RMSE) between the inputs of the original controller and the approximated DNN in the target domain. For the case of zero MPC trajectory, $\pi_\theta = 0$ is applied for calculating the RMSE value.

where $u_{\text{MPC}}(\bar{x}(k))$ and K were designed as same as in the proposed framework. DR baselines collected additional MPC demonstrations around the trajectory $\bar{\xi}$, where sparse sampling was used for DR w/ tube and random sampling within the error tube was used for the conventional DR, respectively. Notably, in these baselines, the DNN alone controlled the cart-pole.

4.1.2 Results: sim-to-real gap

Fig. 5 illustrates the key concept of the proposed framework, showing the controlled cart-pole's position and pole angle in the target domain (Fig. 5a) and the control inputs

Table 1. Comparison of Root Mean Square Error (RMSE).

	Proposed	DR w/ tube	DR (10 Traj.)
RMSE	0.0525	2.263	2.298

generated by the proposed framework and baselines (Fig. 5b). As shown in Fig. 5a, both the proposed method and the DR baselines successfully regulate the cart-pole to the origin, showing aligned results with the original RTMPC, thereby overcoming the sim-to-real gap. This is in contrast to the case when DR is not used (w/o DR), which shows unintended oscillatory results. As shown in Fig. 5b, noisy control inputs were found in the baselines since the DNN handled all disturbances in the target domain. Whereas the DNN in the proposed framework generated cleaner control inputs, as the DNN controls only the nominal model, and the disturbances were compensated by the ancillary controller.

To evaluate performance in dealing with the sim-to-real gap, the Root Mean Squared Error (RMSE) between the DNN's control inputs and the original controller's control inputs that would have resulted in the target domain was analyzed. A smaller value indicates that the DNN represented the original controller better beyond the sim-to-real gap. Fig. 6 shows the RMSE value plotted by the amount of collected data. A total of 100 operations with random disturbances were held and represented as the shaded area, with the average value plotted as the solid line.

The figure shows that the proposed framework resulted in an almost zero RMSE value even with a single demonstrated trajectory since the DNN operates within the source domain. On the other hand, DR baselines required additional perturbations in the source domain, requiring more MPC demonstrations. As shown in Fig. 6, increasing the number of trajectories lowered the RMSE value. However, even with extra data, the DR methods could not match the proposed method's performance, as the sampled disturbances did not fully capture the real disturbances in the target domain. The tube-based DR showed better data efficiency than conventional DR, achieving greater performance with a single trajectory but still exhibiting steady errors for the same reason. Table 1 summarizes the results, confirming that the proposed control structure effectively compensated for the sim-to-real gap while ensuring superior data efficiency compared to the baselines.

4.1.3 Results: model parameter changes

To verify the proposed framework's ability to deal with model parameter changes, further evaluations were held with the changed model parameters in the target domain. The model parameters were set to $M = [6\text{kg}, 0.5\text{kg}]$, differing from the nominal model parameters $\bar{M} = [4\text{kg}, 1\text{kg}]$.

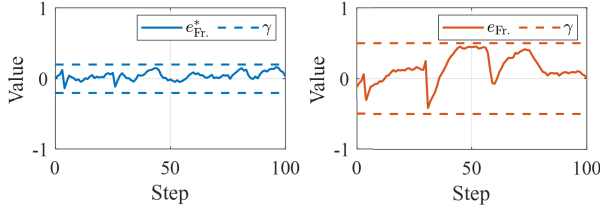


Fig. 7. Required tightening parameter γ with (blue) and without (red) the governor.

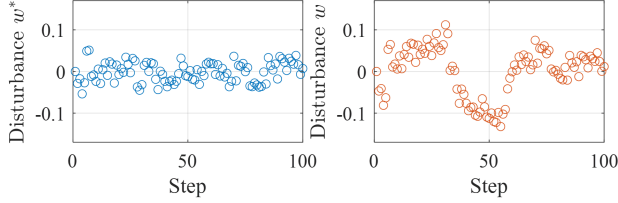
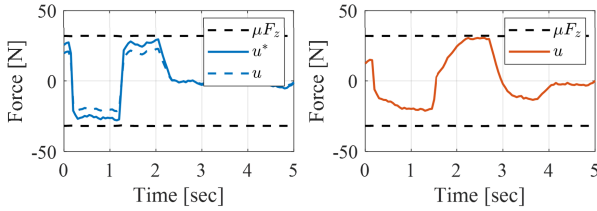
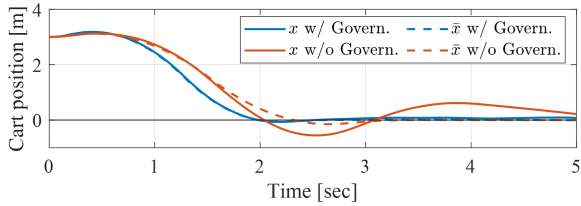


Fig. 8. System disturbance of \dot{x}_{pos} with (blue) and without (red) the governor.



(a) Resulted control inputs with (blue) and without (red) the governor.



(b) Controlled cart position with and without the governor.

Fig. 9. The results of controlled cart position and control inputs with (blue) and without (red) the governor.

The parameter governor accounted for the changed parameters instead of the DNN, refining the control input to satisfy the constraints.

It was verified that the designed governor actually reduced the tightening set. Referring to the derivations of the tightening set in Section 3.3, the tightening parameter γ must be at least bigger than the absolute value of e_g in (21). Therefore, series of $e_{\text{Fr.}}$ and $e_{\text{Fr.}}^*$ were calculated by (21) and (28), respectively:

$$e_{\text{Fr.}}(k) = g_{\text{Fr.}}(x(k), u(k), M) - g_{\text{Fr.}}(\bar{x}(k), \bar{u}(k), \bar{M}) \quad (49a)$$

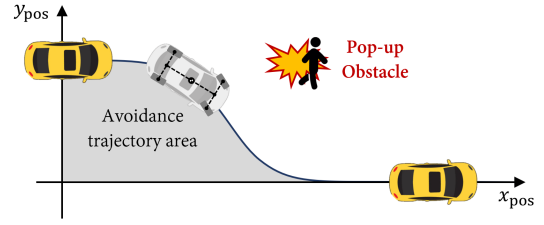


Fig. 10. Vehicle collision avoidance system.

$$e_{\text{Fr.}}^*(k) = g_{\text{Fr.}}(x(k), u^*(k), M) - g_{\text{Fr.}}(\bar{x}(k), \bar{u}(k), \bar{M}) \quad (49b)$$

which is shown in Fig. 7. Without the proposed governor, the tightening parameter $\gamma = 0.5$ was required, meaning that a very conservative MPC using only 50% of the friction limit should be imitated to satisfy the MPC's constraint for the changed model parameters in the target domain. On the other hand, with the proposed governor, $\gamma = 0.2$ was sufficient, allowing for a less conservative MPC to be imitated that utilizes 80% of the friction limit, significantly improving control performance.

In more detail, the refined input reduced the system disturbances, meaning that the proposed governor satisfied the condition of (37). Fig. 8 shows the disturbances encountered in the target domain for the cart position \dot{x}_{pos} during control with and without the governor. Applying the refined control input reduced the system disturbances, therefore, by Proposition 3, the proposed governor is guaranteed to reduce the tightening set as verified in Fig. 7.

Fig. 9 shows the resulted cart position (Fig. 9b) and the control inputs (Fig. 9a) with and without the governor. As shown in Fig. 9a, the governor increased the control input to match the cart-pole's increased mass, demonstrating that the proposed structure can overcome the DNN's limitation of not adapting to model changes. With the governor, a less conservative MPC could be imitated, whereas, without it, a highly conservative MPC was needed, resulting in an overly conservative DNN. Fig. 9b shows the cart-pole's position, confirming the proposed concept where the actual state follows the nominal state controlled by the DNN. With the governor, the cart-pole reaches its origin much faster, as a less conservative MPC was imitated. Also, because the system disturbances were reduced by the governor, smaller deviations between the nominal and actual states were shown.

4.2. Vehicle collision avoidance system

A practical application to a vehicle collision avoidance control case is also studied using CarSim, a high-fidelity vehicle simulation. As shown in Fig. 10, the control objective is to regulate the lateral position of the vehicle to the safe lane (origin) to avoid collision while preventing front tires' saturation to maintain vehicle maneuverability. To

achieve this, an MPC was designed, followed by imitation learning. The compositions of the MPC, nominal prediction model, cost function, and constraints are briefly explained since it is not the main core of this paper. Details can be found in [6].

The system dynamics for the vehicle can be given by:

$$\dot{x}_v = f_v(x_v, u_v) \quad (50a)$$

$$x_v = [x_{\text{pos}}, y_{\text{pos}}, \psi, \dot{\psi}, \beta, v_x]^T \quad (50b)$$

$$u_v = [F_{x,fl}, F_{x,fr}, F_{x,rl}, F_{x,rr}, \delta]^T \quad (50c)$$

using a nonlinear full-car model with a brush tire model [22]. x_{pos} and y_{pos} are the global longitudinal and lateral positions of the vehicle; ψ is the yaw angle; β is the slip angle; v_x is its longitudinal velocity; δ is the front steering angle. F_x and F_y are the longitudinal and lateral forces, respectively, acting on each tire. The subscripts fl , fr , rl , and rr represent the front left, front right, rear left, and rear right tires, respectively. Also, input lags inherited in the lower controllers can be considered as a first-order linear system as follows:

$$\tau_{F_x} \dot{F}_{x,j} = -F_{x,j} + F_{x,j}^{\text{in}}, \text{ for } j = fl, fr, rl, rr \quad (51a)$$

$$\tau_{\delta} \dot{\delta} = -\delta + \delta^{\text{in}} \quad (51b)$$

where τ_{F_x} and τ_{δ} are the time constants for the lower controllers, and $F_{x,j}^{\text{in}}$ and δ^{in} are the control variables.

The control objective is to regulate y_{pos} of the vehicle to the origin to avoid collision. To formulate the MPC's optimization problem, the nominal prediction model was made, derived from (50), (51), as follows:

$$x(k+1) = f(x(k), u(k), \bar{M}) \quad (52a)$$

$$x = [x_v, u_v]^T \quad (52b)$$

$$u = [F_{x,fl}^{\text{in}}, F_{x,fr}^{\text{in}}, F_{x,rl}^{\text{in}}, F_{x,rr}^{\text{in}}, \delta^{\text{in}}]^T \quad (52c)$$

with vehicle parameters $M = [m, I_z, l_f, h, C_y]$ representing vehicle mass m , moment of inertia I_z , distance of the CG point from the front axle l_f , CG height h , and tire's normalized cornering stiffness C_y . A cost function for collision avoidance was structured, which maximizes the space between the vehicle and the obstacle by penalizing the avoidance trajectory area:

$$J(x(k), U(k)) = \sum_{i=0}^{N-1} (q_{\text{avoid}}(x_{i|k}) + u_{v,i|k}^T R_1 u_{v,i|k} + \Delta u_{v,i|k}^T R_2 \Delta u_{v,i|k}) \quad (53)$$

with positive definite matrices R_1 , R_2 for penalizing the control inputs, and $q_{\text{avoid}}(\bullet)$ penalizing the avoidance trajectory area using mensuration by parts as follows:

$$q_{\text{avoid}}(x_{i|k}) = |y_{\text{pos},i|k} v_{x,i|k} \cos(\psi_{i|k} + \beta_{i|k}) T|. \quad (54)$$

Table 2. Initial Conditions for Collecting u_{nom} Demonstrations.

State	Range	State	Range
x_{pos} [m]	0	y_{pos} [m]	2, 3, 4
ψ [deg]	-3, 0, 3	$\dot{\psi}$ [deg/s]	-2, 0, 25
β [deg]	-0.5, 0, 0.5	v_x [km/h]	70, 80, 90
F_x [N]	-1000, 0	δ [deg]	-1, 0, 1

Finally, constraints were applied to ensure vehicle maneuverability by preventing the front tires' grip saturation:

$$\frac{\sqrt{(F_{x,j,i|k})^2 + (F_{y,j,i|k})^2}}{\mu F_{z,j,i|k}} - 1 \leq -\gamma \quad (55)$$

for $j = fl, fr$ and $\forall i = 0, 1, \dots, N-1$.

Note that $0 \leq \gamma \leq 1$ is the tightening parameter. Additional constraints were added to keep braking forces negative, avoid exceeding tire grip, prevent lane departure, and enforce a terminal constraint to ensure y_{pos} converges to the origin, guaranteeing controller stability.

4.2.1 Proposed control framework

By imitation learning, the designed MPC was approximated to a fully connected DNN, with 5 hidden layers of 45 nodes per each. MPC demonstrations were collected from \mathcal{S}_{nom} , starting from various initial states as Table 2. F_x and δ represent the initial driver inputs when the DNN intervenes to avoid collisions, in which the braking forces are distributed across the axles by a factor of η via the proportional valve:

$$F_{x,fl} = F_{x,fr} = F_x \quad (56a)$$

$$F_{x,rl} = F_{x,rr} = \eta F_x \quad (56b)$$

Consequently, a total of 102,060 demonstrations were collected and trained to the DNN.

The ancillary controller was designed as a full-state feedback controller, with an LQR gain K obtained by solving DARE for the linear longitudinal and lateral vehicle model equations to stabilize the X and Y position errors. Under the proposed framework, the control input $u(k)$ was formulated as:

$$u(k) = \pi_{\theta_{\text{Snom}}}(\bar{x}(k)) + K(x(k) - \bar{x}(k)) \quad (57)$$

Finally, for the parameter governor, Proposition 2 leads to the following form regarding the front tires' grip constraints (55):

$$g_{\text{Grip},j}(x(k), M) = g_{\text{Grip},j}(x(k), \bar{M}), \text{ for } j = fl, fr \quad (58)$$

with $g_{\text{Grip},j}(\bullet)$ representing the front tires' grip defined as:

$$g_{\text{Grip},j}(x(k), M) = \frac{\sqrt{(F_{x,j})^2 + (F_{y,j})^2}}{\mu F_{z,j}} \Big|_{(k)} - 1. \quad (59)$$

The proposed governor can be interpreted as matching the front tires' grip of the plant vehicle to the values intended by the DNN, considering the changed vehicle parameters. Then, the refined input u^* satisfying (58) can be obtained by solving the following equation, which is a way to match the longitudinal and lateral normalized forces of each wheel:

$$h_{\text{Grip}}(x(k), M) = h_{\text{Grip}}(\bar{x}(k), \bar{M}) \quad (60)$$

where $h_{\text{Grip}}(\bullet)$ is defined as:

$$h(x(k), M) = \left[\frac{F_{x,fl}}{\mu F_{z,fl}}, \frac{F_{x,fr}}{\mu F_{z,fr}}, \frac{F_{x,rl}}{\mu F_{z,rl}}, \frac{F_{x,rr}}{\mu F_{z,rr}}, \frac{F_{y,f}}{\mu F_{z,f}} \right]^T \bigg|_{(k)} \quad (61)$$

with $F_{y,f}/\mu F_{z,f}$ denoting the normalized lateral tire forces for the front axes, which share identical values for the left and right tires by the brush tire model. Similar to the cart-pole case study, the governor can be physically interpreted as refining the longitudinal and lateral tire forces proportionally to changes in the normal force; that is, if the vehicle mass increases, the braking forces of each wheel increase accordingly, and if the tire parameters changes (cornering stiffness), the steering angle input is refined matching the normalized lateral tire force.

However, due to the delay in the lower actuator (51), the refined input $u^*(k)$ at step k is delayed and impacts $x(k+1)$ at step $k+1$, that is, it is not possible to compute $u^*(k)$ at step k to satisfy (60). Therefore, the governor is designed to compute $u^*(k)$ such that (60) is satisfied in the predicted states at step $k+1$:

$$h_{\text{Grip}}(x_{1|k}^*, M) = h_{\text{Grip}}(\bar{x}_{1|k}, \bar{M}) \quad (62)$$

where $x_{1|k}^*$ and $\bar{x}_{1|k}$ are the one-step predicted states, which can be obtained using the vehicle model as follows:

$$x_{1|k}^* = f(x(k), u^*(k), M) \quad (63a)$$

$$\bar{x}_{1|k} = f(\bar{x}(k), u(k), \bar{M}) \quad (63b)$$

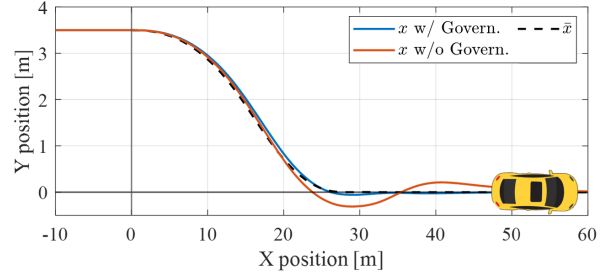
An E-class sedan was controlled in the CarSim target domain, from $y_{\text{pos}} = 3.5\text{m}$ to $y_{\text{pos}} = 0\text{m}$ at 90km/h on a straight road with vehicle parameters M set differently from the nominal parameters \bar{M} as Table 3. Note that the scenario was not included in the conditions for training the DNN, shown in Table 3, and the DNN was only trained to control the nominal vehicle model with nominal parameters \bar{M} in the source domain.

4.2.2 Results

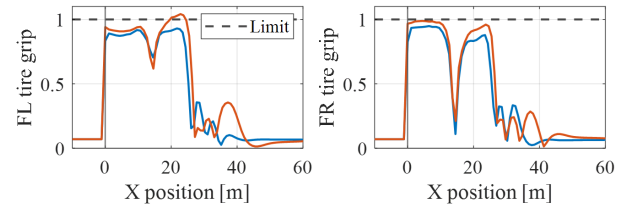
Fig. 11 shows the controlled vehicle position (Fig. 11a) and front tires' grip usage (Fig. 11b) with and without the governor using the same DNN controller. Overall, the proposed controller addressed the sim-to-real gap effectively,

Table 3. Nominal and Actual Vehicle Parameters.

	m [kg]	I_z [kg · m ²]	l_f [m]	h [m]	C_y [—]
\bar{M}	1830	3771	1.41	0.51	17.6
M	+9.2%	+10.6%	+9.2%	+8.3%	+18%



(a) Controlled vehicle position.



(b) Front tires' grip usage.

Fig. 11. Controlled vehicle position and front tires' grip usage with and without the governor.

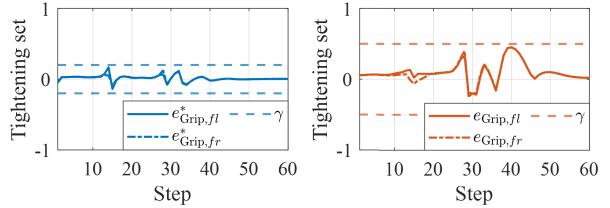


Fig. 12. Required tightening parameter γ with (blue) and without (red) the governor.

controlling the vehicle as the DNN intended in the target domain by following the nominal state, as shown in Fig. 11a. It is also noteworthy that successful control was enabled by a simple behavior cloning-based imitation learning without using advanced methods such as DAGger [23] because the proposed framework enabled the DNN to stay within the source domain.

On the other hand, the controller without the governor made the control inputs just for the trained nominal model parameters and failed to generate control inputs suitable for the changed vehicle parameters. Therefore, the front tires' grip exceeded the limit, leading to tire saturation and reflecting unstable vehicle maneuvers during the evasion, as shown in Fig. 11b. These findings demonstrate

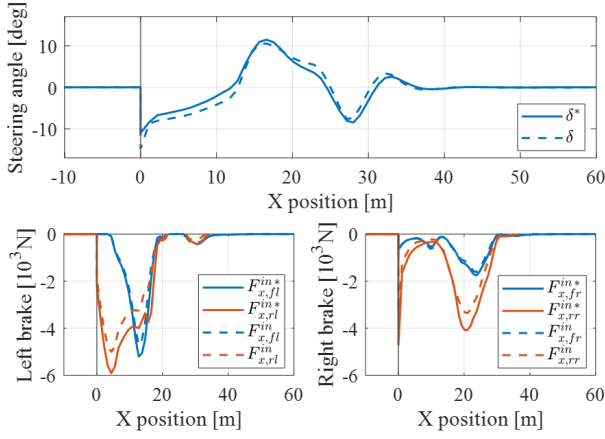


Fig. 13. Control inputs with (blue) and without (red) the governor.

that more conservative tightening is required to deal with the vehicle parameter changes in the target domain when the governor is not used.

Fig. 12 shows the series of $e_{\text{Grip},j}^*(k)$ and $e_{\text{Grip},j}$ for $j = fl, fr$ which were calculated by (21) and (28), respectively. With the proposed governor, tightening parameter $\gamma = 0.1$ was sufficient for the tires' grip constraints, fully utilizing the vehicle's handling limits by using 90% of the front tires' grip. However, without the governor, the tightening parameter $\gamma = 0.5$ was required, meaning that a very conservative MPC using only 50% of the tire grip should be imitated to satisfy the MPC's constraint for the changed vehicle parameters in the target domain, which would significantly degrade the avoidance performance.

Fig. 13 shows the details of the refined control inputs by the governor. Braking force inputs were increased to account for the increased mass and inertia m, I_z and changes in CG positions l_f, h by considering the normal forces of each wheel. Similarly, steering angle inputs were decreased to account for the increased cornering stiffness C_y . Therefore, the grip constraints were satisfied, as shown in Fig. 11a, ensuring vehicle maneuverability during the evasion. As mentioned in the cart-pole example, the governor overcame the DNN's limitations of not adapting to vehicle parameter changes, enabling a less conservative MPC to be imitated.

5. CONCLUSION AND FUTURE WORK

This study proposed a novel control framework to address the sim-to-real gap when applying imitation learning to MPC. Inspired by RTMPC, the DNN is composed of a nominal controller operating in the same environment as the source domain. Compared to DR baselines, the proposed method achieved better data efficiency. Additionally, a parameter governor was introduced to refine the

control input based on changes in model parameters, allowing a less conservative MPC to be imitated.

In this study, two case studies of applying the proposed framework were shown by a cart-pole and a vehicle collision avoidance system example, offering a pathway for generalizing the proposed framework to other control problems. However, the proposed governor is in a highly constrained form, making it still challenging to apply to general control cases. Therefore, for future work, we plan to relax the governor form and validate it in wider control applications.

CONFLICT OF INTEREST

The researchers claim no conflicts of interest.

REFERENCES

- [1] S. Kim, J. Lee, K. Han, and S. B. Choi, "Vehicle path tracking control using pure pursuit with mpc-based look-ahead distance optimization," *IEEE Transactions on Vehicular Technology*, vol. 73, no. 1, pp. 53–66, 2023.
- [2] B. Karg and S. Lucia, "Efficient representation and approximation of model predictive control laws via deep learning," *IEEE transactions on cybernetics*, vol. 50, no. 9, pp. 3866–3878, 2020.
- [3] A. Reske, J. Carius, Y. Ma, F. Farshidian, and M. Hutter, "Imitation learning from mpc for quadrupedal multi-gait control," in *2021 IEEE International Conference on Robotics and Automation (ICRA)*. IEEE, 2021, pp. 5014–5020.
- [4] T. Zhang, G. Kahn, S. Levine, and P. Abbeel, "Learning deep control policies for autonomous aerial vehicles with mpc-guided policy search," in *2016 IEEE international conference on robotics and automation (ICRA)*. IEEE, 2016, pp. 528–535.
- [5] S. Park, D. G. Nguyen, Y. Jin, J. Park, D. Kim, J. S. Eo, and K. Han, "Deep neural network-based approximation of nonlinear model predictive control: Applications to truck-trailer control system," *International Journal of Control, Automation and Systems*, vol. 23, no. 2, pp. 510–519, 2025.
- [6] S. Kim, K. Han, and S. B. Choi, "Imitation learning of nonlinear model predictive control for emergency collision avoidance," *IEEE Transactions on Intelligent Vehicles*, vol. 9, no. 1, pp. 2908–2922, 2023.
- [7] W. Zhao, J. P. Queralta, and T. Westerlund, "Sim-to-real transfer in deep reinforcement learning for robotics: a survey," in *2020 IEEE symposium series on computational intelligence (SSCI)*. IEEE, 2020, pp. 737–744.
- [8] A. Farahani, S. Voghoei, K. Rasheed, and H. R. Arabnia, "A brief review of domain adaptation," *Advances in data science and information engineering: proceedings from ICDATA 2020 and IKE 2020*, pp. 877–894, 2021.
- [9] A. Allevato, E. S. Short, M. Pryor, and A. Thomaz, "Tunenet: One-shot residual tuning for system identification and sim-to-real robot task transfer," in *Conference on Robot Learning*. PMLR, 2020, pp. 445–455.

- [10] O. M. Andrychowicz, B. Baker, M. Chociej, R. Jozefowicz, B. McGrew, J. Pachocki, A. Petron, M. Plappert, G. Powell, A. Ray *et al.*, “Learning dexterous in-hand manipulation,” *The International Journal of Robotics Research*, vol. 39, no. 1, pp. 3–20, 2020.
- [11] D. Wada, S. Araujo-Estrada, and S. Windsor, “Sim-to-real transfer for fixed-wing uncrewed aerial vehicle: pitch control by high-fidelity modelling and domain randomization,” *IEEE Robotics and Automation Letters*, vol. 7, no. 4, pp. 11 735–11 742, 2022.
- [12] J. Wang, Y. Liu, and B. Li, “Reinforcement learning with perturbed rewards,” in *Proceedings of the AAAI conference on artificial intelligence*, vol. 34, no. 04, 2020, pp. 6202–6209.
- [13] J. Tobin, R. Fong, A. Ray, J. Schneider, W. Zaremba, and P. Abbeel, “Domain randomization for transferring deep neural networks from simulation to the real world,” in *2017 IEEE/RSJ international conference on intelligent robots and systems (IROS)*. IEEE, 2017, pp. 23–30.
- [14] J. Tremblay, A. Prakash, D. Acuna, M. Brophy, V. Jampani, C. Anil, T. To, E. Cameracci, S. Boochoon, and S. Birchfield, “Training deep networks with synthetic data: Bridging the reality gap by domain randomization,” in *Proceedings of the IEEE conference on computer vision and pattern recognition workshops*, 2018, pp. 969–977.
- [15] H. Tsukamoto and S.-J. Chung, “Learning-based robust motion planning with guaranteed stability: A contraction theory approach,” *IEEE Robotics and Automation Letters*, vol. 6, no. 4, pp. 6164–6171, 2021.
- [16] A. Tagliabue and J. P. How, “Efficient deep learning of robust policies from mpc using imitation and tube-guided data augmentation,” *IEEE Transactions on Robotics*, 2024.
- [17] H. Hose, A. Gräfe, and S. Trimpe, “Parameter-adaptive approximate mpc: Tuning neural-network controllers without retraining,” in *6th Annual Learning for Dynamics & Control Conference*. PMLR, 2024, pp. 349–360.
- [18] I. V. Kolmanovsky and J. Sun, “Parameter governors for discrete-time nonlinear systems with pointwise-in-time state and control constraints,” *Automatica*, vol. 42, no. 5, pp. 841–848, 2006.
- [19] J. B. Rawlings, D. Q. Mayne, M. Diehl *et al.*, *Model predictive control: theory, computation, and design*. Nob Hill Publishing Madison, WI, 2017, vol. 2.
- [20] J. Lee and S. B. Choi, “Integrated control of steering and braking for path tracking using multi-point linearized mpc,” *IEEE Transactions on Intelligent Vehicles*, vol. 8, no. 5, pp. 3324–3335, 2022.
- [21] J. Lee, Y. Hwang, and S. B. Choi, “Robust tube-mpc based steering and braking control for path tracking at high-speed driving,” *IEEE Transactions on Vehicular Technology*, vol. 72, no. 12, pp. 15 301–15 316, 2023.
- [22] H. Pacejka, *Tire and vehicle dynamics*. Elsevier, 2005.
- [23] S. Ross, G. Gordon, and D. Bagnell, “A reduction of imitation learning and structured prediction to no-regret online learning,” in *Proceedings of the fourteenth international conference on artificial intelligence and statistics*. JMLR Workshop and Conference Proceedings, 2011, pp. 627–635.



Seungtaek Kim received the B.S. degree in Mechanical Engineering from Yonsei University, Seoul, South Korea, in 2019, and the M.S. and Ph.D. degrees in Mechanical Engineering from Korea Advanced Institute of Science and Technology (KAIST), Daejeon, Korea, in 2021 and 2025, respectively. Since 2025, he is currently working as a Postdoctoral Research Fellow in KAIST. His research interests include vehicle dynamics and control, control theory, and imitation learning.



Jonhyup Lee received the B.S., M.S., and Ph.D. degrees in Mechanical Engineering from Korea Advanced Institute of Science and Technology (KAIST), Daejeon, Korea, in 2015, 2017, and 2023, respectively. From 2023 to 2024, he was with Hyundai Motor Company as a Senior Research Engineer. Since 2024, he has been with the Department of Mechanical Systems Engineering at Sookmyung Women’s University, Seoul, Korea, as an Assistant Professor. His research interests include autonomous driving decision and control, vehicle dynamics and control, and control theory.



Kyoungseok Han received his B.S. degree in Civil Engineering with a minor in Mechanical Engineering from Hanyang University, Seoul, South Korea, in 2013, followed by M.S. and Ph.D. degrees in Mechanical Engineering from KAIST, Daejeon, South Korea, in 2015 and 2018, respectively. He is currently an Associate Professor in the Department of Automotive Engineering at Hanyang University, Seoul, South Korea. Prior to this, he worked as a Postdoctoral Research Fellow at the University of Michigan from 2018 to 2020 and as an Associate Professor at Kyungpook National University, Daegu, South Korea from March 2020 to August 2024. His research interests include autonomous vehicle modeling and control, energy-efficient control of electric vehicles, reinforcement learning, and optimal control theory and its applications.



Seibum B. Choi received a B.S. in Mechanical Engineering from Seoul National University, Seoul, Korea, an M.S. in Mechanical Engineering from KAIST, Daejeon, Korea, and a Ph.D. in control from the University of California, Berkeley, CA, USA, in 1993. From 1993 to 1997, he was involved in developing automated vehicle control systems at the Institute of Transportation Studies, University of California.

Through 2006, he was with TRW, Livonia, MI, USA, where he was involved in developing advanced vehicle control systems. Since 2006, he has been faculty in the Mechanical Engineering Department of KAIST, Korea. His research interests include fuel-saving technology, vehicle dynamics and control, and active safety systems. Prof. Choi is a Member of the American Society of Mechanical Engineers, the Society of Automotive Engineers, and the Korean Society of Automotive Engineers.

Publisher's Note Springer Nature remains neutral with regard to jurisdictional claims in published maps and institutional affiliations.